# Cobalt Oxalate Nanoribbons as Negative-Electrode Material for Lithium-Ion Batteries

María José Aragón, Bernardo León, Carlos Pérez Vicente, and José L. Tirado*

*Laboratorio de Química Inorgánica, Universidad de Córdoba, Edificio C3, Campus de Rabanales, 14071 Córdoba, Spain*

Alan V. Chadwick, Aaron Berko, and See-Yuen Beh

*Functional Materials Group, School of Physical Sciences, University of Kent, Canterbury, Kent CT2 7NR, U.K.*

*Received October 15, 2008. Revised Manuscript Received March 11, 2009*

Orthorhombic cobalt oxalate dihydrate has been prepared in the form of nanoribbons by a reverse micelles method. The crystallographic structure of the resulting solid differs from the monoclinic massive product. A careful dehydration of the nanocrystals leads to anhydrous cobalt oxalate in which the nanoribbon-shaped particles are preserved and $Co^{2+}$ ions are located in a centrosymmetric environment. $CoC_2O_4$ is used for the first time as high-capacity lithium storage materials with improved rate performance. The anhydrous solids react with lithium, leading to metallic cobalt and lithium oxalate, as shown by XAS and FTIR measurements. The new electrode material displays reversible capacities close to 900 $mA \cdot h \cdot g^{-1}$ between 0 and 2 V versus lithium by a novel reaction mechanism which involves cobalt reduction−reoxidation.

## Introduction

Recently, hundreds of new compounds never imagined to be active electrode materials in lithium batteries have been proven to display interesting reversible reactions with lithium. A variety of reaction types are involved, such as intercalation, alloying, conversion, or displacement, which occur in different regions of a wide potential interval from 0 V to ∼5 V versus lithium. Many of these "new" electrode materials achieve their activity by their preparation in the form of nanomaterials, which allows intimate contact with the electrolyte and shortens the chemical diffusion lengths during the electrochemical reaction. Some examples include elements,[1] hydrides,[2] fluorides,[3] oxides,[4,5] nitrides,[6] phosphides,[7] and oxysalts,[8,9] some of them providing capacities of several thousands of $mA \cdot h \cdot g^{-1}$ in the case of anodes and hundreds for the cathodes. Simultaneous to the discovery of new materials, a precise understanding of reaction mechanisms has been acquired. Particularly, conversion electrodes involving transition metal oxides, and more recently, transition metal fluorides, show a reduction of the metal ions to the metallic state together with the formation of lithium oxide or lithium fluoride, respectively. These reactions lead to highly dispersed reaction products. In addition, the initial control on the dispersion of the reagents may improve the response of most electrode materials. Both aspects taken together emphasize that lithium battery materials are particularly attractive in the field of nanoscience and nanotechnology.

We are examining the possibility of extending the range of new materials to submicrometric particles of transition metal oxysalt. Previous studies revealed that $MnCO_3$ and $FeC_2O_4$ can be used directly as a conversion electrode versus lithium.[8,9] The discharge of lithium test cells takes place by a different conversion reaction than that observed for the oxide produced during the thermal decomposition of the oxysalts, MnO and FeO.

In this work, the study of different forms—bulk and nano—of cobalt oxalate is carried out to discover the usefulness of this oxysalt as anode material for advanced lithium-ion batteries. Besides the known drawbacks in the use of cobalt compound—cost, availability, and toxicity—cobalt is still an element difficult to replace in the lithium-ion technology. In fact, it is in the early successful $LiCoO_2$ and the more recent $LiCo_{1/3}Ni_{1/3}Mn_{1/3}O_2$ cathodes, and in the anode of the commercial Sony Nexelion products.[10] The preparation routes of cobalt oxides and cobalt−tin alloys are commonly time- and energy-consuming. In this paper we examine the use of cobalt oxalate, a common and

* To whom correspondence should be addressed. E-mail: iq1ticoj@uco.es. Phone: +34957218637.

(1) Chan, C. K.; Peng, H.; Liu, G.; McIlwrath, K.; Zhang, X. F.; Huggins, R. A.; Cui, Y. *Nat. Nanotechnol.* **2008**, *3*, 31–35.
(2) Oumellal, Y.; Rougier, A.; Nazri, G. A.; Tarascon, J. M.; Aymard, L. *Nat. Mater.* **2008**, *7*, 916–921.
(3) Badway, F.; Mansour, A. N.; Pereira, N.; Al-Sharab, J. F.; Cosandey, F.; Plitz, I.; Amatucci, G. G. *Chem. Mater.* **2007**, *19*, 4129–4141.
(4) Poizot, P.; Laruelle, S.; Grugeon, S.; Tarascon, J. M. *J. Electrochem. Soc.* **2002**, *149*, A1212−A1219.
(5) Alcántara, R.; Jaraba, M.; Lavela, P.; Tirado, J. L. *Chem. Mater.* **2002**, *14*, 2847–2848.
(6) Cabana, J.; Stoeva, Z.; Titman, J. J.; Gregory, D. H.; Palacin, M. R. *Chem. Mater.* **2008**, *20*, 1676–1678.
(7) Alcántara, R.; Tirado, J. L.; Jumas, J. C.; Monconduit, L.; Olivier-Fourcade, J. *J. Power Sources* **2002**, *109*, 308–312.
(8) Aragón, M. J.; Pérez-Vicente, C.; Tirado, J. L. *Electrochem. Commun.* **2007**, *9*, 1744–1748.
(9) Aragón, M. J.; León, B.; Pérez-Vicente, C.; Tirado, J. L. *Inorg. Chem.* **2008**, *47*, 10366–10371.
(10) Press release, http://www.sony.net/SonyInfo/News/Press/200502/05-006E/, Feb 15, 2005 (accessed Dec 2005)

10.1021/cm803435p CCC: $40.75 
Published on Web 04/06/2009

inexpensive compound as compared to the ceramic cobalt oxides, as a high-capacity electrode.

## Experimental Section

Two samples of cobalt(II) oxalate were considered in this study. Commercial cobalt oxalate (Panreac, Barcelona) was used as-received. A second sample was synthesized by a reverse micelles procedure from water-in-oil microemulsions, as follows: First, two microemulsions (I and II) were obtained under an argon atmosphere. Microemulsion I contained cetyl-trimethylammonium bromide (CTAB) as the surfactant, hexanol as the cosurfactant, isooctane as the hydrocarbon phase, and 0.3 M cobalt(II) nitrate solution as the aqueous phase. Microemulsion II has the same constituents as above except for having 0.3 M ammonium oxalate instead of cobalt nitrate as the aqueous phase. The weight fractions of the various constituents in these microemulsions are as follows: 16.76% CTAB, 13.9% hexanol, 59.29% isooctane, and 10.05% aqueous phase. In a second step, both microemulsions were slowly mixed and stirred overnight on a magnetic stirrer. The resulting precipitate was separated from the apolar solvent and surfactant by centrifugation followed by rinsing with a 1:1 mixture of methanol and chloroform. The different hydrated cobalt oxalate particles were subjected to a careful thermal decomposition at 200 °C under vacuum to yield anhydrous $CoC_2O_4$.

X-ray diffraction (XRD) patterns were recorded on a Siemens D5000, using Cu Kα radiation and a graphite monochromator. Scanning electron microscopy (SEM) and transmission electron microscopy (TEM) images were obtained in a JEOL JSM63000 microscope and JEOL 200CX microscope, respectively. Thermogravimetric (TG) and differential thermal analysis (DTA) curves were obtained in a Shimadzu DTG-60AH instrument. $N_2$ adsorption isotherms at 77 K were obtained with a Quantachrome instrument.

For electrochemical tests, two-electrode Swagelok-type lithium test cells were used. The electrodes were prepared by blending the powdered active material (60%) with carbon black (30%) and poly vinylidene fluoride (10%) dissolved in *N*-methyl-pyrrolidone. The weight of active material in the electrodes for cycling experiments was about 3 mg, and the electrode was 9 mm in diameter. The slurry was cast onto a Cu foil and vacuum-dried at 120 °C. As the negative electrode, a lithium foil was used. The electrolyte was a solution of ethylene carbonate−diethyl carbonate in 1:1 weight proportion, including 1 M $LiPF_6$, supported by a porous glass-paper disk. The cells were assembled/disassembled in an Ar-filled glovebox ($H_2O$, $O_2$ < 1 ppm). Galvanostatic charge/discharge cycles were carried out at different *C* rates ($C$ = 1 $Li \cdot h^{-1} \cdot mol^{-1}$, i.e., ~0.22 $mA \cdot cm^{-2}$ current density). Charge/discharge experiments were interrupted at selected voltages and the electrodes removed without relaxation period for spectroscopic and diffraction examination. Step potential electrochemical spectra were obtained at different sweep rates.

XANES measurements in the Co K edge were carried out on station 9.3 at the SRS at Daresbury. The measurements were performed in normal transmission mode using gas-filled ion chambers. A third ion chamber was used to collect the XAS of a metal foil placed after the signal ion chamber. This provided a reference for the calibration of the edge position for each scan. The synchrotron energy is 2 GeV, and the average ring current during the experiments was 150 mA. The energy scales were calibrated taking as the zero the Co K edge of Co (7710 eV). Used electrodes were kept inside a thermosealed bag (Aldrich) inside the dry box, and the bag was directly transferred to the XAS station. In addition to the electrode material, XAS spectra were collected for Co metal, CoO, and $Co_3O_4$, as reference materials for the XANES analysis. The data were processed in the conventional manner using the Daresbury suite of EXAFS programs: EXCALIB, EXBACK, and EXCURV98.[11] Phase shifts were derived from ab initio calculations within EXCURV98.

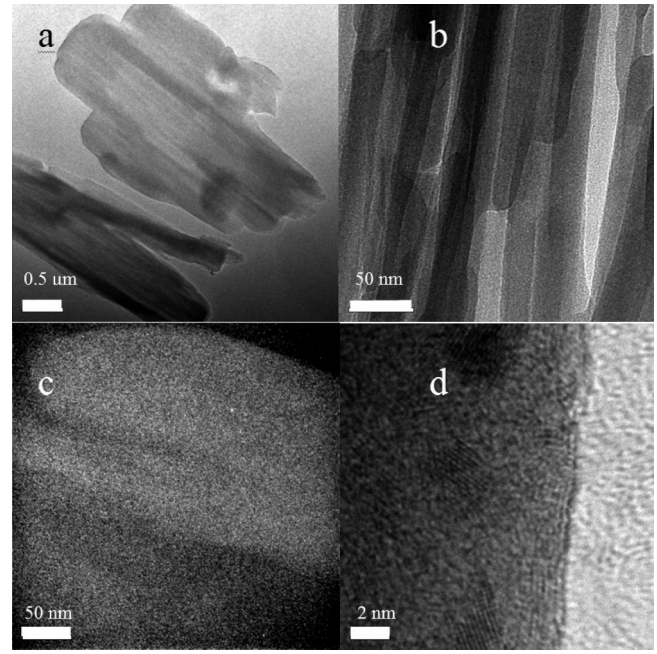


**Figure 1.** TEM images of dehydrated cobalt oxalate: (a,c) commercial and (b,d) micellar material.

## Results and Discussion

The XRD patterns of commercial and micellar $CoC_2O_4 \cdot 2H_2O$ (see Supporting Information, Figure S1) exhibited significantly different diffractograms. As in other transition metal oxalates, cobalt oxalate dihydrate was shown early to crystallize into two allotropic forms: α monoclinic, space group *C*2/*c*, and β orthorhombic, *Cccm*.[12] For commercial cobalt oxalate, the pattern could be indexed in a monoclinic lattice with $a = 11.814_9$ Å, $b = 5.587_8$ Å, $c = 9.858_2$ Å, and $\beta = 128.56_3°$, in good agreement with a high-purity α form, according to the description by Deyrieux et al. ($a$ = 11.775 Å, $b$ = 5.416 Å, $c$ = 9.859 Å, and $\beta$ = 127.85°).[12] In contrast, the oxalate synthesized by the reverse micelles procedure showed the reflections ascribable to an orthorhombic lattice with $a = 11.920_9$ Å, $b = 5.431_8$ Å, and $c = 15.521_1$ Å, also in good agreement with literature values for the $\beta$-$CoC_2O_4 \cdot 2H_2O$ phase ($a$ = 11.877 Å, $b$ = 5.419 Å, and $c$ = 15.624 Å).[12]

TEM micrographs of the commercial and micellar dihydrated oxalates also showed significant differences (Figure 1). Irregularly shaped particles of several micrometers were visible for the commercial product, whereas nanoribbons ~30 nm wide are observed for the sample obtained using reverse micelles. These results emphasize the effectiveness of the

(11) (a) Binsted, N.; Campbell, J. W.; Gurman, S. J.; Stephenson, P. C. *SERC Daresbury Program Library*; Daresbury Laboratory: Warrington, Cheshire, U.K., 1992. (b) Binsted, N. *EXCURV98: CCLRC Daresbury Laboratory computer program*; CCLRC Daresbury Laboratory: Warrington, Cheshire, U.K., 1998.
(12) Deyrieux, R.; Berro, C.; Peneloux, A. *Bull. Soc. Chim. Fr.* **1973**, *12*, 25–34.

reverse micelles procedure to obtain nanoparticles with controlled size and shape. The presence of the surfactant molecules during the precipitation reaction avoids the contact between the particles of the reaction products. The origin of the elongated shape in cobalt oxalate, and in other transition metal oxalate dihydrate nanoparticles,[9,13,14] can be ascribed to anisotropic structure of the solid.

Thermogravimetric curves (see Supporting Information, Figure S2) confirmed that both cobalt oxalate samples crystallize with two water molecules. The curves were useful in locating the temperature at which the two water molecules are released from $CoC_2O_4 \cdot 2H_2O$ without breakage of the oxalate anion. After the initial weight loss of adsorbed water up to 120 °C, the observed weight losses up to 200 °C (18.6% for the commercial sample and 18.9% for the micellar sample) are in good agreement with the theoretical value (19.7%) according to eq 1:

$$CoC_2O_4 \cdot 2H_2O \rightarrow CoC_2O_4 + 2H_2O \quad (1)$$

Following dehydration, at temperatures larger than 200 °C, a second weight loss effect is visible in the TG curves (45.3% commercial and 42.8% micellar referred to the weight of the anhydrous $CoC_2O_4$), which is ascribable to oxalate decomposition, according to both eq 2 in an inert atmosphere and eq 3 in the presence of traces of oxygen (both with 45% of theoretical loss), which globally account for the main exotherm in the DTA curve and the weight loss at 270 °C.[15]

$$3CoC_2O_4 \rightarrow Co_3O_4 + 4CO + 2CO_2 \quad (2)$$

$$3CoC_2O_4 + {}^1/_2O_2 \rightarrow Co_3O_4 + 3CO + 3CO_2 \quad (3)$$

The TG data of the dehydrated products obtained at 200 °C under static vacuum for 8 h (Figure S2) also showed weight losses of 45.9% and 44.5%, in good agreement with eq 2. Irrespective of the origin of the oxalate sample and the crystallographic structure of the starting solid, the XRD patterns of the dehydrated products (Figure S1) showed a small number of highly broadened reflections which agreed well with a poorly crystalline solid with a $CoC_2O_4$ composition. A solid with this composition has been studied in ref 16 in which the cobalt ions were shown to be in an octahedral coordination.[16]

The dehydrated product resulting from the commercial sample retained both the micrometric particle size and the heterogeneous particle size and shape of the hydrated precursor. TEM micrographs of the dehydrated micellar oxalate (Figure 1) showed that the nanometric particles with elongated shapes were preserved during dehydration. However, the nanoribbons ~30 nm wide observed for the sample obtained using reverse micelles contain smaller domains, revealed by their lattice fringes (Figure 1d).

Figure 2 shows the first few galvanostatic cycles of lithium test cells using $CoC_2O_4$ as active electrode material. For both commercial and micellar samples, the first discharge at 2C took place with a first extended plateau at ~1 V versus Li, followed by a steeper region up to ~1400 $mA \cdot h \cdot g^{-1}$ at 0 V. The electrodes were recycled in the plateau region, where mostly irreversible electrolyte reactions were found (Figure 2). Nevertheless, a rechargeable component of 150−200 $mA \cdot h \cdot g^{-1}$ is observed, which is indicative of the starting of reversible processes in this voltage range. As commonly found in conversion electrodes, the initial irreversible capacity is large, and the Faradaic nature of this process is discussed below. Further cycles displayed up to 900 $mA \cdot h \cdot g^{-1}$ reversible capacities, which is significantly higher than the theoretical capacity of graphite (372 $mA \cdot h \cdot g^{-1}$). From Figure 2c it is clear that the contribution of the additives is almost negligible. The voltage profile agrees well with that previously reported for $FeC_2O_4$.[9] The discharge process leads to an X-ray amorphous product after the first discharge, the crystallinity of which was not recovered during additional charge−discharge cycles. Analogous to previous conversion electrode materials, the first step could be associated with the formation of cobalt metal, according to

$$CoC_2O_4 + 2Li^+ + 2e^- \rightarrow Co + Li_2C_2O_4 \quad (4)$$

XAS was used to confirm this hypothesis, as shown below. The theoretical capacity value calculated for reaction 4 is 365 $mA \cdot h \cdot g^{-1}$. Thus, there is a huge extra irreversible capacity that could be ascribed to both the formation of a SEI and extended electrolyte degradation. This agrees with the larger irreversible capacity for the nanometric micellar particles. As compared with other oxysalts previously studied,[8,9] the values are higher and this effect has to be avoided for a practical application of these electrode materials. The differences with $FeC_2O_4$ and $MnCO_3$ could be a consequence of a different catalytic effect of the different transition metal nanoparticles.[17] The reversible capacity values for the oxalate also contrast markedly with the theoretical capacity of reaction 4. Different origins of this discrepancy could be the following: The possible reversible formation of an "organic" layer such as that described by Tarascon and co-workers[18] enhanced by the composition of the composite material (cobalt metal and lithium carboxylates), or a contribution of capacitative effects, which are particularly favored by the Ultrafine texture of the oxalate particles, and especially by the presence of Ultrafine cobalt particles.

X-ray absorption near edge structure (XANES) spectroscopy is a particularly well-suited technique for providing deep insight into the oxidation state of the absorber atoms.

(13) Pujol, O.; Bowen, P.; Stadelmann, P. A.; Hofmann, H. *J. Phys. Chem. B* **2004**, *108*, 13128–13136.
(14) Vaidya, S.; Rastogi, P.; Agarwal, S.; Gupta, S. K.; Ahmad, T.; Antonelli, A. M.; Ramanujachary, K. V.; Lofland, S. E.; Ganguli, A. K. *J. Phys. Chem. C* **2008**, *112*, 12610–12615.
(15) MacKenzie, R. C. *Differential Thermal Analysis*; Academic Press: New York, 1970; p 401.
(16) Nikonenko, E. A.; Sharov, V. A.; Olikov, I. I.; Zhdanovskikh, T. M. *Z. Neorg. Khim.* **1982**, *27*, 975–979.
(17) Kang, Y.-M.; Song, M.-S.; Kim, J.-H.; Kim, H.-S.; Park, M.-S.; Lee, J.-Y.; Liu, H. K.; Dou, S. X. *Electrochim. Acta* **2005**, *50*, 3667–3672.
(18) Débart, A.; Dupont, L.; Poizot, P.; Leriche, J.-B.; Tarascon, J. M. *J. Electrochem. Soc.* **2001**, *148*, A1266−A1274.
(19) Nakai, I.; Takahashi, K.; Shiraishi, Y.; Nakagome, T.; Izumi, F.; Ishii, Y.; Nishikawa, F.; Konishi, T. *J. Power Sources* **1997**, *68*, 536–542.
(20) Yoon, W. S.; Kim, K. B.; Kim, M. G.; Lee, M. K.; Shin, H. J.; Lee, J. M.; Lee, J. S.; Yo, C. H. *J. Phys. Chem. B* **2002**, *106*, 2526.

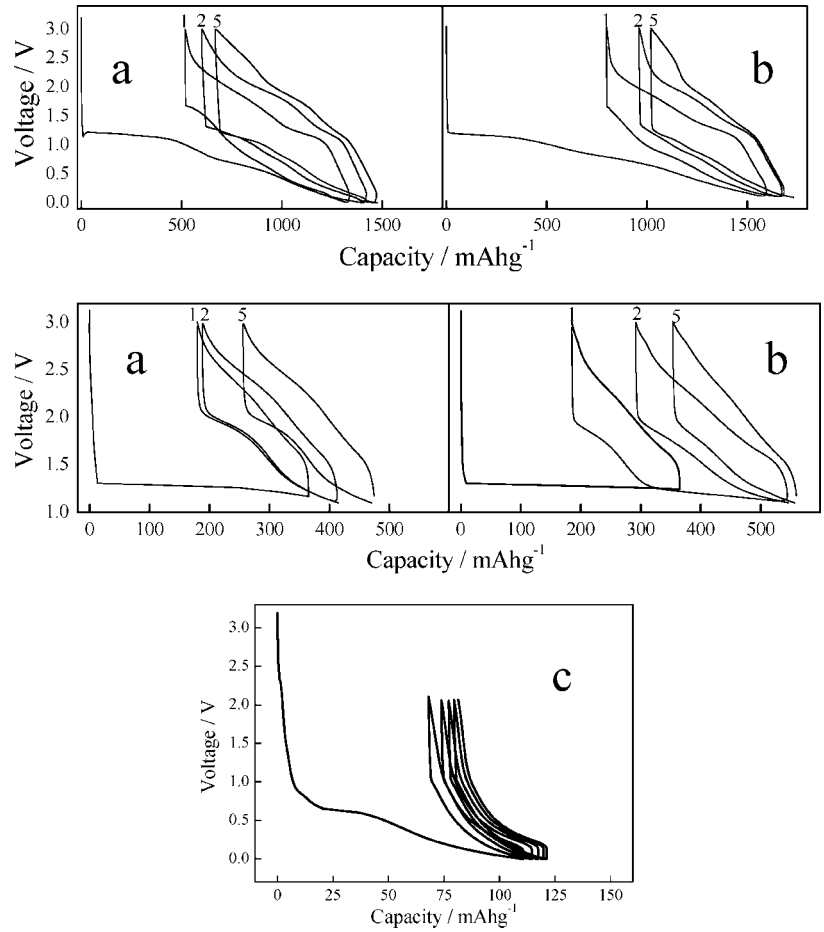


**Figure 2.** Charge−discharge branches of lithium test cells at 2C in two voltage ranges (upper curves, 0.01−3.0 V; lower curves, 1.1− 3.0 V) for (a) commercial and (b) micellar dehydrated samples. A blank test (c) is the performance of a cell containing only 75% carbon black and 25% PVdF. The electrolyte was a solution of ethylene carbonate−diethyl carbonate in 1:1 weight proportion, including 1 M $LiPF_6$.

The XAS spectra have been successfully used in the study of $Li_{1-x}CoO_2$ cathode material,[19,20] and cobalt species in lower oxidation states in conversion electrodes.[21,22] Figure 3 shows the normalized CoK-edge XANES of the dehydrated oxalate. The edge features of this spectrum are distinguishable from those of Co(III) (shown for $Co_3O_4$), which clearly indicates the divalent state of cobalt (see the spectrum for CoO). The pre-edge peak resulting from the absorption process 1s → 3d is almost negligible. The transition probability (peak intensity) is related to the coordination symmetry and to the occupancy of the 3d shell of cobalt. In an octahedral symmetry, the transition is forbidden by the center of symmetry, even though a weak pre-edge is commonly observed resulting from the crystallographic distortion and constantly vibrating local environments momentarily eliminating the center of symmetry. In contrast, the pre-edge peak becomes more intense with the noncentrosymmetric environment such as tetrahedral cobalt. Therefore, the weak pre-edge features in Figure 3 for cobalt oxalate may be interpreted as being in a centrosymmetrical coordination. According to Nikonenko et al., the divalent metal in anhydrous $MC_2O_4$ (M: Mn, Fe, Co, Ni, Zn) has an octahedral configuration.[16]

The EXAFS of the dehydrated commercial cobalt oxalate is shown in Figure 4. The Fourier transform exhibits three peaks at ∼2.0, 2.9, and 3.9 Å. Unfortunately, there are no detailed crystallographic data on which to base a model for detailed EXAFS fitting. Intuitively, the first shell around the Co atom will be O and on that basis we fitted the data assuming this shell consisted of six (octahedral) O atoms. The best fit to this model is shown as the dashed line in Figure 4 and yielded a Co−O distance of 2.08 Å. This value is close (within the EXAFS error of ±0.02 Å) to the Co−O distance of 2.095 Å found in catena-poly[[diaquacobalt(II)]-$\mu$-oxalato].[23]

A first step of examining the nature of the reduced products will help gain further insight into the electrochemical reaction that takes place in these electrode materials. The changes in the Co K-edge XANES spectra of the $CoC_2O_4$ electrodes (Figure 3) evidence the displacement of the edge to lower energies throughout the discharge (lithium insertion) process, which is indicative of a cobalt reduction process in $CoC_2O_4$, which leads to metallic cobalt and $Li_2C_2O_4$ on approaching 0 V. Nevertheless, the spectra at 0 V is not exactly coincident

(21) Chadwick, A. V.; Savin, S. L. P.; Alcántara, R.; Fernández Lisbona, D.; Lavela, P.; Ortiz, G. F.; Tirado, J. L. *ChemPhysChem* **2006**, *7*, 1086–1091.

(22) Chadwick, A. V.; Savin, S. L. P.; Fiddy, S.; Alcántara, R.; Fernández Lisbona, D.; Lavela, P.; Ortiz, G. F.; Tirado, J. L. *J. Phys. Chem. C* **2007**, *111*, 4636–4642.

(23) Bacsa, J.; Eve, D.; Dunbar, K. R. *Acta Crystallogr.* **2005**, *C61*, m58–m60.

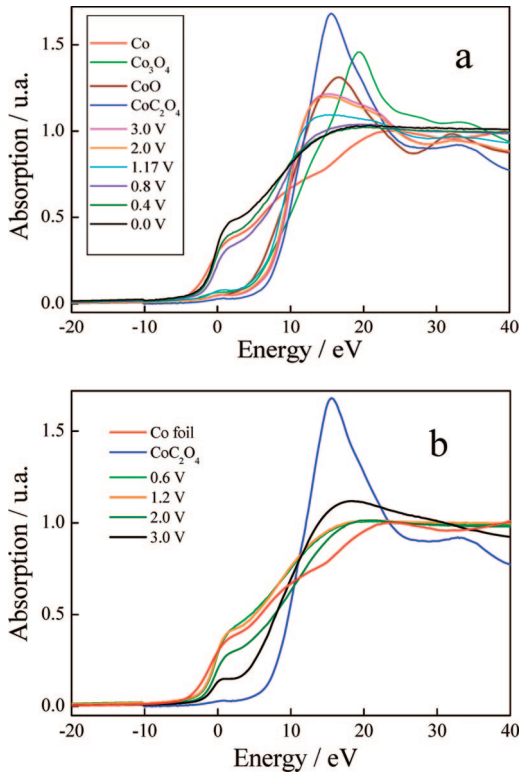


**Figure 3.** CoK XANES spectra of dehydrated commercial cobalt oxalate electrodes n lithium test cell. (a) During discharge. (b) During cell charge. The XANES of model compounds are included for comparison.

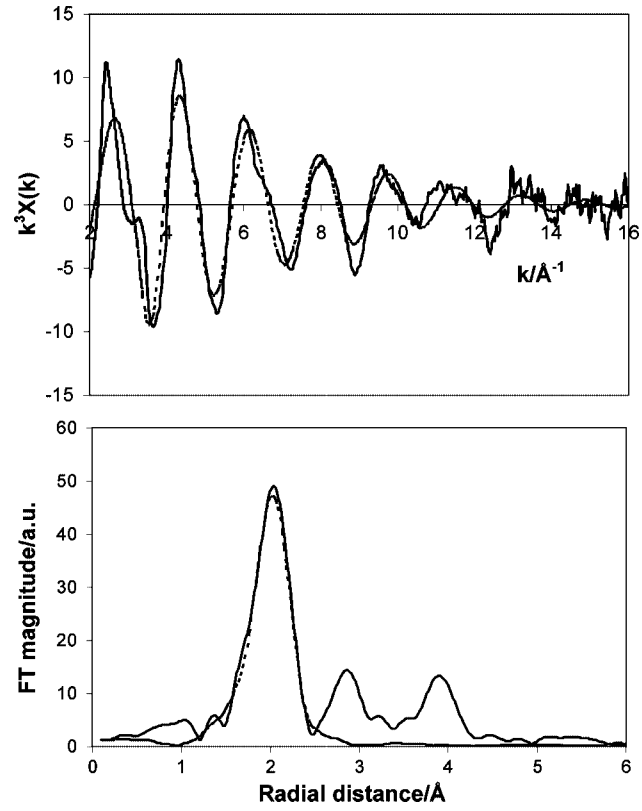


**Figure 4.** Co K-edge EXAFS for the dehydrated commercial cobalt oxalate. The upper curve is the normalized EXAFS. The lower curve is the Fourier transform corrected with the phase shift of an oxygen first shell. The solid line is the experiment and the dashed line is the best fit (see text).

with that of crystalline Co foil because of the contribution of surface atoms in the nanodispersed product, as found in previous studies.[21,22] Two steps can be distinguished during the discharge process in Figure 3a. From 3.0 to ∼1.17 V, the XANES spectra do not alter markedly. Probably in that voltage interval, which coincides with the insertion of ca. 0.5 F mol$^{-1}$ of $CoC_2O_4$, the changes are mostly related to irreversible reactions with the electrolyte and SEI formation. From 2.0 to 0.0 V, Figure 3a reveals a progressive loss of signal intensity of the white line. This behavior can be related to the loss of p character in the 1s → 4p transition, due to d−p mixing, as a consequence of the conversion to metal cobalt particles, absorbing X-rays at the lower energy values.

The Fourier transforms of the EXAFS collected at various points of the discharge are shown in Figure 5. To make comparisons possible, we used the same phase shift (a first shell of Co atoms) for all the transforms and marked the positions of the first shells for dehydrated cobalt oxalate and cobalt metal. We see that as the discharge voltage decreases, there is a relative growth of the peak corresponding to metallic cobalt, although the absolute magnitude for this peak does not change uniformly. However, the magnitude of this peak is much smaller than that for the cobalt metal foil. Our previous study of $NiCo_2O_4$ electrodes on lithium insertion[21] gave similar results and is indicative that the metallic cobalt is in the form of very small nanoparticles.

The XANES spectra obtained after recharge of the lithium cells using $CoC_2O_4$ electrodes are shown in Figure 3b. The reversibility of the reduction process is evidenced after lithium extraction up to 1.5 V by the fact that the spectra partially recover their shape. However, the +2 oxidation state of cobalt atoms in the dehydrated oxalate is not fully recovered, as shown by the position of the edge. This behavior agrees with the nonrecovered irreversible capacity observed in Figure 2. After charge to 1.5−3.0 V, some differences from the starting $CoC_2O_4$ are observed. Thus, the prepeak at lower energy is more clearly observed than that in $CoC_2O_4$. Also, the most intense peak is located at lower energy. Thus, the structure of the oxidized material differs from the initial oxalate structure and less symmetric environments of cobalt are expected. It is worth noting that the reoxidation process is progressive in contrast to what was observed during the first discharge, thus anticipating the reversibility of further cycles.

In addition, FTIR data were obtained to check the integrity of oxalate ions in the used electrodes. The experimental spectra of used electrodes are collected in the Supporting Information (Figure S3). The presence of oxalate ions can be derived by the band at ∼1320 cm$^{-1}$, which is characteristic of both $CoC_2O_4$ and $Li_2C_2O_4$. This effect is present in the used electrodes but is absent in the electrolyte, which confirms that oxalate ions are preserved on cycling. Thus, it can be concluded that the system is close to previous study on iron oxalate but differs significantly from conventional conversion oxide electrodes, as the matrix formed during the discharge is lithium oxalate instead of lithium oxide.

The following cycles were found to be reversible. Figure 6 shows the rate performance of cobalt oxalate. The initial capacity is significantly lower at a high rate, whereas extended cycling reveals excellent capacity retention for 5C. Consequently, the values observed at 50 cycles or higher

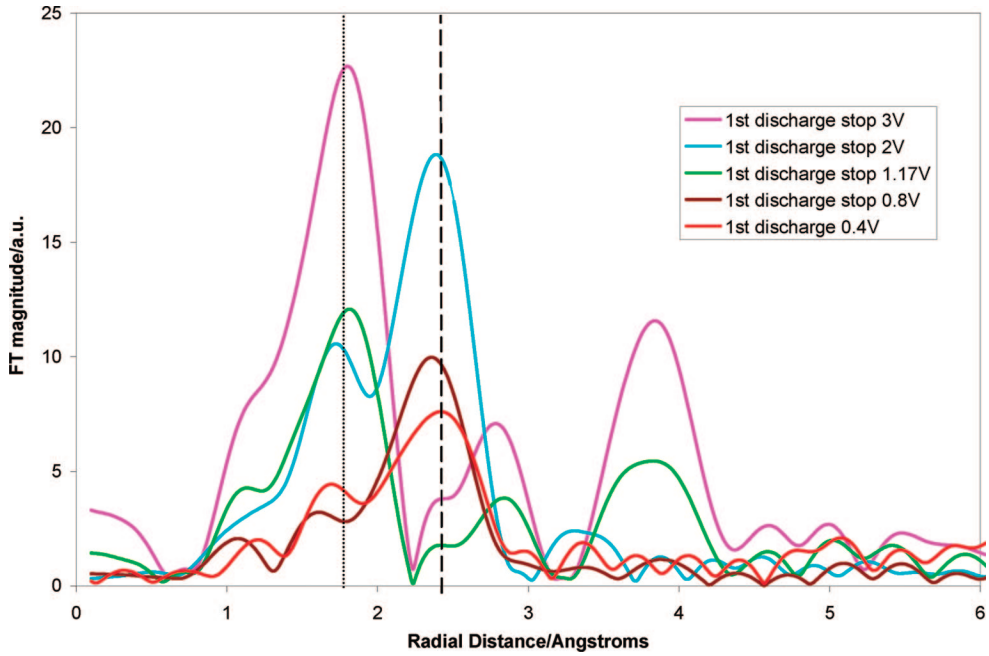


**Figure 5.** Fourier transform Co K-edge EXAFS samples of dehydrated commercial cobalt oxalate electrodes during discharge. The transforms were corrected with the phase shift of cobalt atoms in the first shell. The dotted line corresponds to the first shell position in dehydrated cobalt oxalate. The dashed line corresponds to the first shell position in cobalt metal.

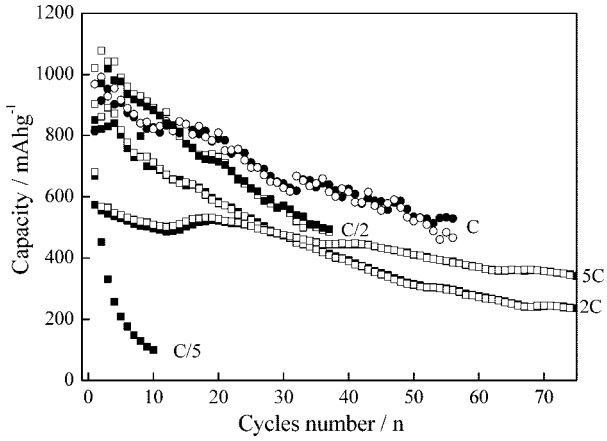


**Figure 6.** Capacity vs cycle number in the 0.01−3.0 V potential window of lithium cells using commercial $CoC_2O_4$ electrode materials at different rates.

are rather close for the different rates. At present, we have no clear explanation for the discrepancy between C and C/5 rates in Figure 6. However, this fact inspires extra interest in these materials as high-rate electrodes.

The XANES spectra after successive charges and discharges are shown in Figure 7. The spectra for the charged electrodes are all very similar and agree with the presence of $Co^{2+}$ ions. For discharged electrodes the position of the edge is similar in all cycles, suggesting the presence of cobalt metal. However, there are differences in the shapes of the XANES region, which might be due to differences in the surrounding environment of the cobalt-containing nanoparticles. Then it can be concluded that these results agree with the previous interpretation of $Co^0$(noncentrosymmetric)−$Co^{2+}$(centrosymmetric) conversions.

Returning to Figure 2, the charge−discharge branches display significant hysteresis phenomena, a feature which is commonly observed, and limits the use of conversion

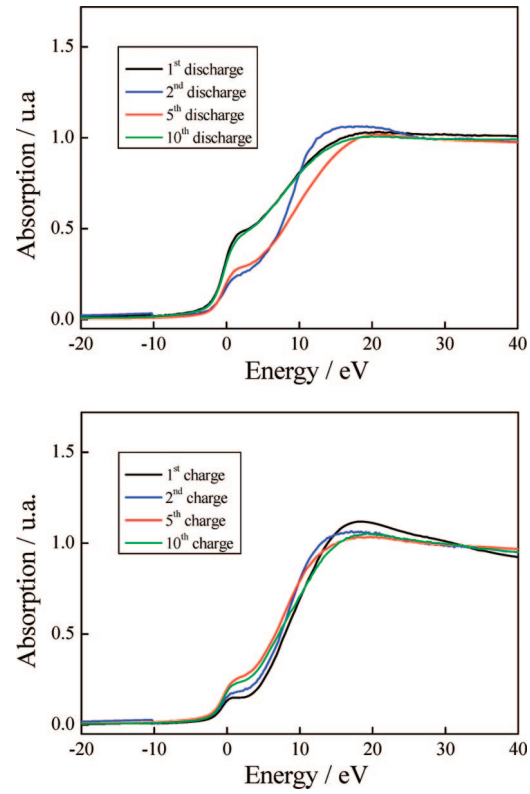


**Figure 7.** XANES of dehydrated commercial cobalt oxalate cycled electrodes in the 0.01−3.0 V potential window.

electrodes. To further examine the origin of the hysteresis phenomena, the differences in cell potential of the charge and discharge branches ($\Delta E$) were plotted against the C rate (equivalent to current density for constant sample weights; see Supporting Information Figure S4). When the rate is increased, an enhanced cell potential difference is seen. This pattern results in a straight line when plotted in a logarithmic scale (square symbols), which is indicative of Arrhenius

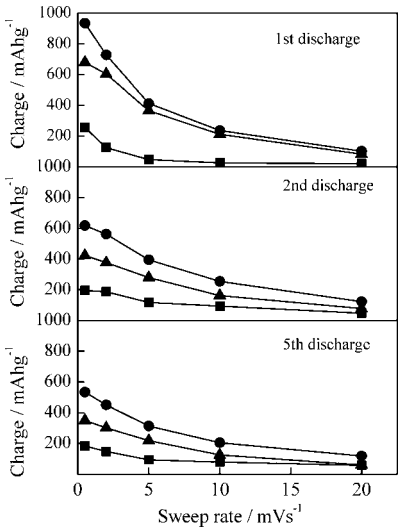


**Figure 8.** Capacity vs sweep rate in step-potential electrochemical spectroscopy discharges of dehydrated commercial cobalt oxalate electrodes in the 0.01−3.0 V potential window for discharges 1, 2, and 5. Circles, total capacity; triangles, Faradaic capacity; squares, non-Faradaic capacity.

behavior. These results agree well with an excellent study on the electrochemical behavior of another conversion electrode, $Fe_3O_4$, which was found to behave as impedance with an activation step and not as pure resistance.[24] The reaction is then governed by mass transfer through grain boundaries between the three solid-state components during the charge/discharge processes. The differences in the slope of the plots between cobalt oxalate and iron oxide suggest that one of the solid-state components is lithium oxalate instead of $Li_2O$, with different ion mobility.

To understand the origin of the extra capacity from the theoretical value of the pure conversion reaction (4), we have carried out a study of the possible contribution of Faradaic and non-Faradaic (capacitance) to the global observed values. This study follows the model recently described by Brezesinski et al. for $TiO_2$ electrodes.[25] The results are shown in Figure 8. It is clear that the first discharge is mostly Faradaic and irreversible and overpasses the theoretical capacity. The contribution of irreversible reactions with the electrolyte are demonstrated. On further cycles, the Faradaic capacity gets closer to the theoretical capacity of the proposed conversion reaction, while the extra capacity comes from non-Faradaic origin.

The electrochemical behavior in lithium test cells of $CoC_2O_4 \cdot 2H_2O$ polycrystalline samples in both allotropic forms was poor. In contrast, the cyclability of both dehydrated oxysalts was significantly improved. The results for

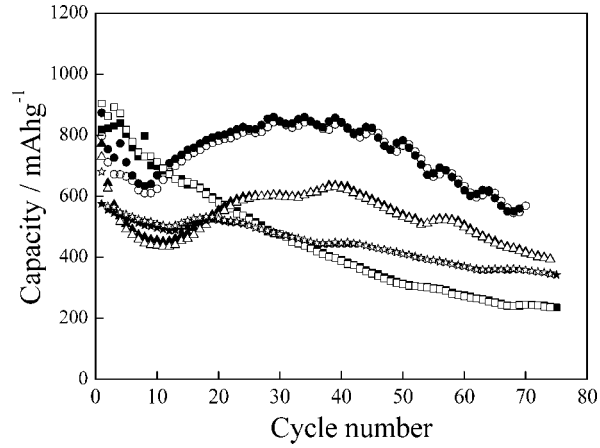


**Figure 9.** Capacity vs cycle number in the 0.01−3.0 V potential window of lithium cells using $CoC_2O_4$ electrode materials at different C rates: circles, micellar sample, 2C; triangles, micellar, 5C; squares, commercial, 2C; and stars, commercial, 5C. Filled symbols, discharge values; hollow symbols, charge values.

both $CoC_2O_4$ samples are compared in Figure 9. Even cycling at higher rate, micellar cobalt oxalate shows higher capacity than the solid resulting from commercial $CoC_2O_4 \cdot 2H_2O$. Moreover, the capacities are higher than those previously reported for manganese carbonate[8] and iron oxalate.[9]

## Conclusions

The main conclusion of this study is that anhydrous cobalt oxalate nanoparticles are potential candidates for the active material of the negative electrode of lithium-ion batteries. The low-temperature dehydration synthesis of this solid could lower production costs as compared with other successful cobalt-based electrodes. As compared with other materials, the cobalt has a superior performance in lithium test cells, with reversible capacities above 900 $mA \cdot h \cdot g^{-1}$, and good capacity retention at high rates. As compared with a commercial product, a higher capacity is observed for ribbon-like nanoparticles obtained by the reverse micelles procedure. Nevertheless, the complexity of the synthesis of the micellar product may not compensate for the increase in capacity. In both cases, the hysteresis phenomena, which are common to conversion electrodes, could limit the practical application of these materials.

**Acknowledgment.** The authors are indebted to EC (ALISTORE), MEC (MAT2008-05880), and Junta de Andalucía (FQM288). S.Y.B. is grateful to EC for her ERASMUS MUNDUS grant.

**Supporting Information Available:** This material is available free of charge via the Internet at http://pubs.acs.org.

CM803435P

(24) Taberna, P. L.; Mitra, S.; Poizot, P.; Simon, P.; Tarascon, J. M. *Nat. Mater.* **2006**, *5*, 567–577.
(25) Brezesinski, T.; Wang, J.; Polleux, J.; Dunn, B.; Tolbert, S. H. *J. Am. Chem. Soc.* **2009**, *131*, 1802–1809.